



Geophysical Research Letters

RESEARCH LETTER

10.1029/2020GL091478

Key points:

- Sea surface salinity drops after passing of Tropical Depressions and Storms, with minima to the left of the storm track
- Above hurricane force, post-storm salinification dominates to the right, with higher magnitude for intense slowly-moving storms
- Pre-storm upper ocean vertical salinity gradients control haline and thermal wakes. River plumes exhibit the strongest salinity wakes

Supporting Information:

- Supporting Information S1

Correspondence to:

N. Reul,
nicolas.reul@ifremer.fr.

Citation:

Reul, N., Chapron, B., Grodsky, S. A., Guimbard, S., Kudryavtsev, V., Foltz, G. R., & Balaguru, K. (2021). Satellite observations of the sea surface salinity response to tropical cyclones. *Geophysical Research Letters*, 48, e2020GL091478. <https://doi.org/10.1029/2020GL091478>

Received 28 OCT 2020

Accepted 20 NOV 2020

Satellite Observations of the Sea Surface Salinity Response to Tropical Cyclones

Nicolas Reul¹ , Bertrand Chapron¹, Semyon A. Grodsky² , Sébastien Guimbard³, Vladimir Kudryavtsev^{4,5}, Gregory R. Foltz⁶ , and Karthik Balaguru⁷

¹Laboratoire d'Océanographie physique et spatiale, Univ Brest, Ifremer, CNRS, IRD, LOPS, Plouzané, France,

²Department of Atmospheric and Oceanic Science, University of Maryland, College Park, MD, USA, ³OceanScope,

Brest, France, ⁴Satellite Oceanography Laboratory, Russian State Hydrometeorological University, Saint-Petersburg, Russia, ⁵Remote Sensing Department, Marine Hydrophysical Institute, Sevastopol, Russia, ⁶NOAA/Atlantic

Oceanographic and Meteorological Laboratory, Miami, FL, USA, ⁷Pacific Northwest National Laboratory, Seattle, WA, USA

Abstract Decade-long satellite sea surface salinity (SSS) observations show that rain dilution prevails in wakes of tropical depressions (~ -0.1 pss) and tropical storms (~ -0.05 pss) on the left (right) side of Northern (Southern) Hemisphere storms. For stronger storms, the rain-induced dilution is dominated by the saltier water entrainment, leading to surface median salinification of 0.3 pss for the most intense storms, peaking on the right-hand side at around twice the maximum wind radius. The magnitude of the salty wake increases for stronger slowly moving storms. The vertical salinity gradient in the upper ocean is a key factor explaining the geographic distribution of the SSS response. A striking example is the systematic mixing of fresh near-surface river plume waters with saltier subsurface waters. It is also found that barrier layers lead to saltier and warmer storm wakes compared to wakes produced over barrier layer free areas.

Plain Language Summary Tropical cyclones (TCs) generate a well-known cooling of the ocean's surface. However, the response of the ocean's surface salinity to TCs, and the processes involved, are much less known. This response can be a potential indicator of salinity's control on TC-induced ocean cooling: for some storms, stronger TC-induced increases in salinity has been associated with reduced mixing and cooling. Here we show that the salinity response to TCs varies widely depending on the strength and residence time of the TC, the pre-existing vertical salinity structure, and the location relative to the storm's center. Weak storms cause freshening on average, whereas stronger storms generate an increase in salinity. This is in contrast to TC-induced changes in ocean surface temperature, which are always negative (i.e., cooling). Unambiguously, areas with the lowest pre-existing surface salinity (i.e., regions of heavy rainfall and river outflow) have the largest TC-induced increases in surface salinity and experience muted surface cooling.

1. Introduction

The sea surface salinity (SSS) response to tropical cyclone (TC) passage results from TC-induced rainfall, evaporation, deepening of the upper ocean prestorm mixed layer, upwelling of subsurface water, as well as surrounding water mass advection (Ginis, 2002; Robertson & Ginis, 2002).

Poststorm SSS salinification in the trail of TCs has already been extensively reported both from in situ and satellite observations (e.g., see Bond et al., 2011; Chaudhuri et al., 2019; Domingues et al., 2015; Grodsky et al., 2012; Lin et al., 2017; Liu et al., 2020; McPhaden et al., 2009; Price, 1981; Reul et al., 2014; Sanford et al., 1987; Steffen & Bourassa, 2018; Venkatesan et al., 2014; Vinayachandran et al., 2003; Yue et al., 2018; Zhang et al., 2016, 2018). SSS is generally expected to increase in the wakes of cyclones because subsurface water is on average saltier than surface water in the convective regions associated with cyclonic activity (Jourdain et al., 2013). In line with the thermal wake signature, a rightward SSS asymmetry is also anticipated from storm-induced inertial currents in the Northern Hemisphere (Price, 1981). However, heavy precipitations under TCs may lead to poststorm upper ocean freshening, as reported from in situ observations (Bond et al., 2011; Hsu and Ho, 2019; Kil et al., 2013; Lin & Oey, 2016; Lin et al., 2017; Liu et al., 2007, 2020;

Pudov & Petrichenko, 2000; Steffen & Bourassa, 2018; Zhang et al., 2016), and numerical simulations (Jacob & Koblinsky, 2007; Robertson & Ginis, 2002).

Global-scale model-driven analyses (Jourdain et al., 2013) and the North Pacific data composites of Argo float vertical salinity profile response (Lin et al., 2017) still show that on average, near the surface, ocean upwelling and mixing overwhelm the dilution effect of rain freshwater: the cyclone “cold wake” is hence also generally a “salty wake.” For North Pacific typhoons, upper ocean Argo data confirm that the more intense and the slower the storm, or, the shallower the precyclonic Mixed-Layer Depth (MLD), the saltier the SSS responses to TCs (Lin et al., 2017). Contrastingly, Argo data in the Atlantic, Eastern Pacific, and Central Pacific tropical ocean (Steffen & Bourassa, 2018) indicate that TC SSS wakes may be dominated by poststorm mixed-layer freshening. Note, while providing first estimates of the “net” regional impact of TCs on SSS, Argo float profiler network sampling (1 measurement every 10 days over 300 km²) is limited with respect to typical TC characteristic scales both in space (50–600 km, Knaff et al., 2014) and time (several hours to 2–3 days, Hall & Kossin, 2019).

To complement these first studies, we take advantage of the 10-years long period of satellite SSS products to present new insights and to more precisely document the ocean surface salinity response to TC passage, its global “mean” structure and associated variability. From L-band radiometer measurements on-board the Soil Moisture and Ocean Salinity (SMOS) and Soil Moisture Active Passive (SMAP) missions, accurate estimates of some large-amplitude haline surface anomalies left in the wake of TCs have already been successfully demonstrated for several individual TC cases (Chaudhuri et al., 2019; Grodsky et al., 2012; Neethu, 2018; Reul et al., 2014; Yue et al., 2018). SSS retrievals in high wind conditions during the forced stage of TCs remain highly uncertain (Boutin et al., 2018; Meissner et al., 2018; Reul et al., 2020) and are therefore not considered in the present study. While less accurate than in situ observations, the large number of instantaneous SSS measurements that can be collected from these sensors over the last decade can be used to build more robust statistical climatological composites of the SSS response to TCs and its evolution as a function of storm characteristics and environmental conditions. Combined with thermal responses, this 10-years long period can quantify the role upper ocean salinity may play during TC development (see Balaguru et al., 2020, and references herein).

Data and methods are detailed in Section 2. Radial characteristics of the SSS response and its evolution as a function of TC characteristics and pre-storm ocean conditions, as well as the co-variabilities between SSS and sea surface temperature (SST) responses are presented in Section 3. Summary and conclusions are given in Section 4.

2. Data and Methods

Time series of TC center track location, peak 1-min wind speed (V_{\max}), maximum wind radius (R_{\max}), storm center translation speed (V_t), as well as Gale force (34 kt) wind radii in each geographical storm quadrant (R_{34}) are obtained for each TC over 2010–2019 from the International Best Track Archive for Climate Stewardship (IBTrACS, Knapp et al., 2010), data set version v04 (<https://www.ncdc.noaa.gov/ibtracs/>).

Daily global composites of the swath SSS provided on a 25 × 25-km² grid and separated into ascending and descending orbits as retrieved from SMOS (Kerr et al., 2010) and SMAP (Entekhabi et al., 2014, p. 182) satellite missions are considered hereafter. We used the SMOS “L3OS 2Q” products from the Centre Aval de Traitement des Données SMOS (Boutin et al., 2018; CATDS, 2019), available over 2010–2019. SMAP salinity data (August 2015 to December 2019) are the Remote Sensing Systems V4.0 SMAP Level 2C products (Meissner et al., 2018, www.remss.com/missions/smap/). These data provide global coverage within 5 and 3 days at the equator, respectively. Potentially reduced quality retrievals were removed using the ensemble of Quality Control (Q/C) flags available in the products, including local wind speed conditions in excess of 14–15 m/s (Q/C flags’ Bit#12 in SMAP V4.0 and “Fg_sc_high_wind” in SMOS products, respectively). Satellite SSS was therefore collected either before, or after the storm passage, but not during the forced stage.

In addition to SSS, we examine daily 0.09° grid resolution SST based on the Group for High Resolution Sea Surface Temperature (GHRSST) Level 4 Global Foundation Sea Surface Temperature analysis v5.0 (Remote Sensing Systems, 2017).

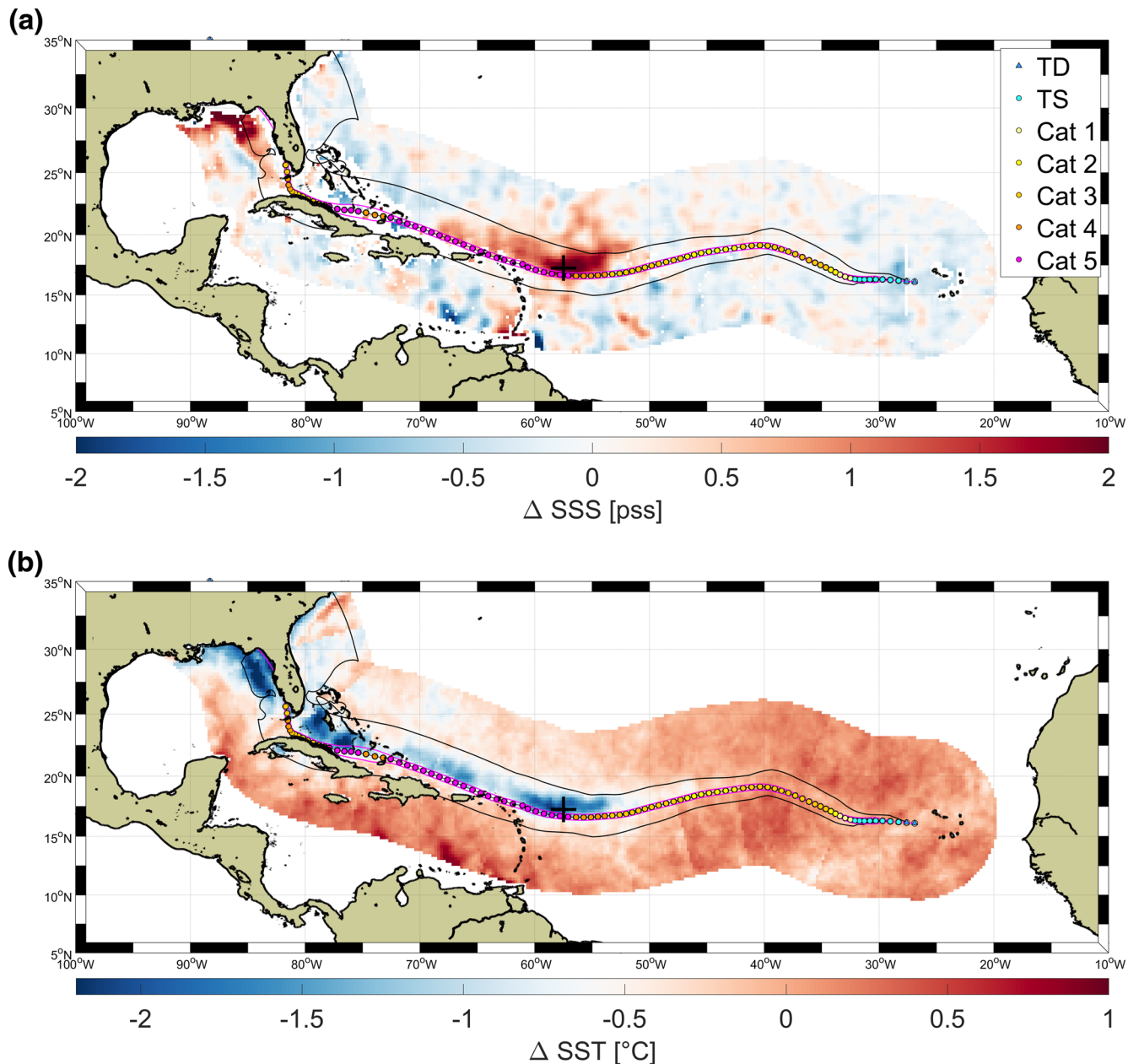


Figure 1. Haline (a) and thermal (b) surface wakes left by Hurricane Irma (2017). The thin black and magenta curves are indicating the 34 kt and maximum wind radii, respectively. The color circles indicate the storm center location and intensity (see legend in (a)).

For each of the 864 storms that developed in all TC basins during 2010–2019, a spatial domain of analysis extending ± 750 km across the storm center track was determined, as illustrated in Figure 1 for Hurricane Irma (2017) in the North Atlantic. SSS and daily SST time series ranging from 20 days before to 40 days after the storm passage were collected at each $0.25 \times 0.25^{\circ}$ grid points within the wake domain, together with the radial distance to storm center track r and the TC main characteristics (V_{\max} , R_{\max} , V_t , R_{34}) at the time of the center's nearest passage. Note that a positive r is associated with the right-hand side (left-hand side) of the track for the Northern (Southern) Hemisphere. Prestorm and poststorm conditions are estimated by averaging data from 10 to 3 days prior, and from 0 to 5 days after the storm, respectively (see Figure S1). In situ 1/2° resolution monthly analyses generated from Argo profilers on 152 vertical levels by the In Situ Analysis System (ISAS-15, Gaillard et al., 2016) are used to estimate prestorm subsurface properties. Vertical salinity S , temperature T , and density ρ are interpolated bi-linearly in time and space from the monthly ISAS fields.

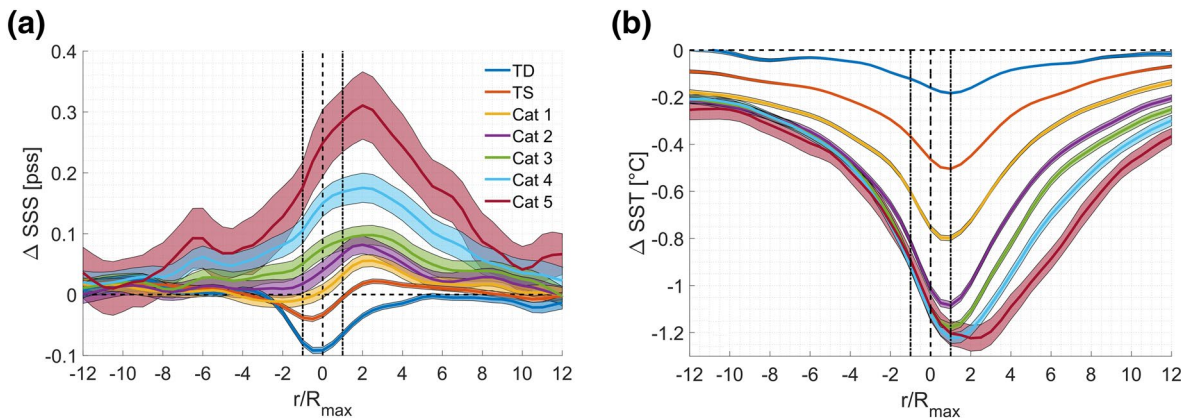


Figure 2. Radial (x -axes) distributions of the median SSS (a) and SST (b) response to TCs as a function of SSWS intensity (color code provided in the legend in (a)). For each intensity, the median (thick black curves) is evaluated in r/R_{\max} bins of width 1/2. The color patches indicate the extent of the 95% confidence intervals. The storm center and the radial borders of the inner eye-wall ($|r/R_{\max}| = 1$) are indicated by black vertical dash lines. SSS, sea surface salinity; SST, sea surface temperature; TC, tropical cyclone; SSWS, Saffir-Simpson Wind Scale.

The prestorm Mixed-Layer Depth (D_σ) and barrier-layer thickness (BLT), estimated as the difference between the isothermal layer (ILD) and the MLD, were determined following De Boyer Montégut et al. (2007). The prestorm salinity S^- and temperature T^- at a depth 5 m below the MLD were also used to evaluate the prestorm mixed-layer vertical salinity gradient $\Gamma_s = (\text{SSS}-S^-)/D\sigma$. Combining SMOS and SMAP SSS data, we collected these quantities for about 8.3×10^6 samples (Figure S2). The results presented here combine SMOS and SMAP databases to increase statistical significance.

3. Results

Figure 2 presents radial sections of the median TC-induced SSS and SST anomalies (denoted ΔSSS and ΔSST hereafter) for each Saffir-Simpson Wind Scale (SSWS) category (Schott et al., 2012). The all-basin median haline response to TC passage exhibits a peak-to-peak amplitude of ~ 0.5 psu over the full range of storm intensities (Figure 2a). To note, after the passage of Tropical Depressions (TD), $\Delta \text{SSS} \leq 0$ systematically emerges on average in their wakes, extending almost entirely across-track and reaching a minimum of about -0.1 psu at $r/R_{\max} \approx -1/2$, i.e., on the left side within the storm inner eye-wall region. For Tropical Storms (TS), a weaker minimum of ~ -0.05 is also detected at $r/R_{\max} \approx -1/2$, but ΔSSS becomes positive for $r/R_{\max} \geq 1$. The poststorm SSS signature then progressively becomes saltier as storm intensity increases. The salty wake maxima are clearly observed to develop on the right-hand side of the storm tracks at about $r/R_{\max} \approx 2$, peaking slightly more rightward than SST cooling minima (at $r/R_{\max} \approx 1-2$, Figure 2b). For intensities above Category 2, wakes are systematically saltier than prestorm almost everywhere within the extent of the Gale force wind region $|r/R_{34}| \leq 1$ (Figure S3), with a monotonic maximum salinity rise as cyclone intensity increases. Contrastingly, as found by Lloyd and Vecchi (2011), the SST response-TC intensity relationship is nonmonotonic with stronger cyclones producing more cooling up to Category 2, but producing approximately equal cooling for Categories 3–5. The spatial distribution of the median SSS anomalies left by TCs is shown in Figure 3a. There is regional variability in the net impact of all TCs on SSS. There are areas dominated by mixed-layer freshening (Arabian Sea, north of Australia, most of the western Pacific, Atlantic north of 20°N, Caribbean Sea, Southwest Indian Ocean). But there are striking signatures of mixing of the fresh surface river plume waters with much saltier subsurface waters (Amazon, Orinoco, Mississippi, Bay of Bengal, and Yangtze). A key factor of the salinity response to TCs is thus the strength of the prestorm vertical salinity gradients in the upper ocean mixed-layer Γ_s . The distribution of Γ_s in the region where TCs develop (Figure 3b) clearly evidences that largest negative Γ_s occurs over the major freshwater surface pools, sourced by either rain (Indonesian waters, eastern Pacific fresh pool, Inter Tropical Convergence Zones), or, by large river discharges. Over other regions, Γ_s is either weakly negative, neutral, or weakly positive ($|\Gamma_s| < 0.01 \text{ m}^{-1}$). As illustrated in Figure 3c, when $\Gamma_s < 0$, the fresher the prestorm SSS with respect to the prestorm salinity just below the MLD, the saltier the SSS response at a fixed TC intensity. To note, for

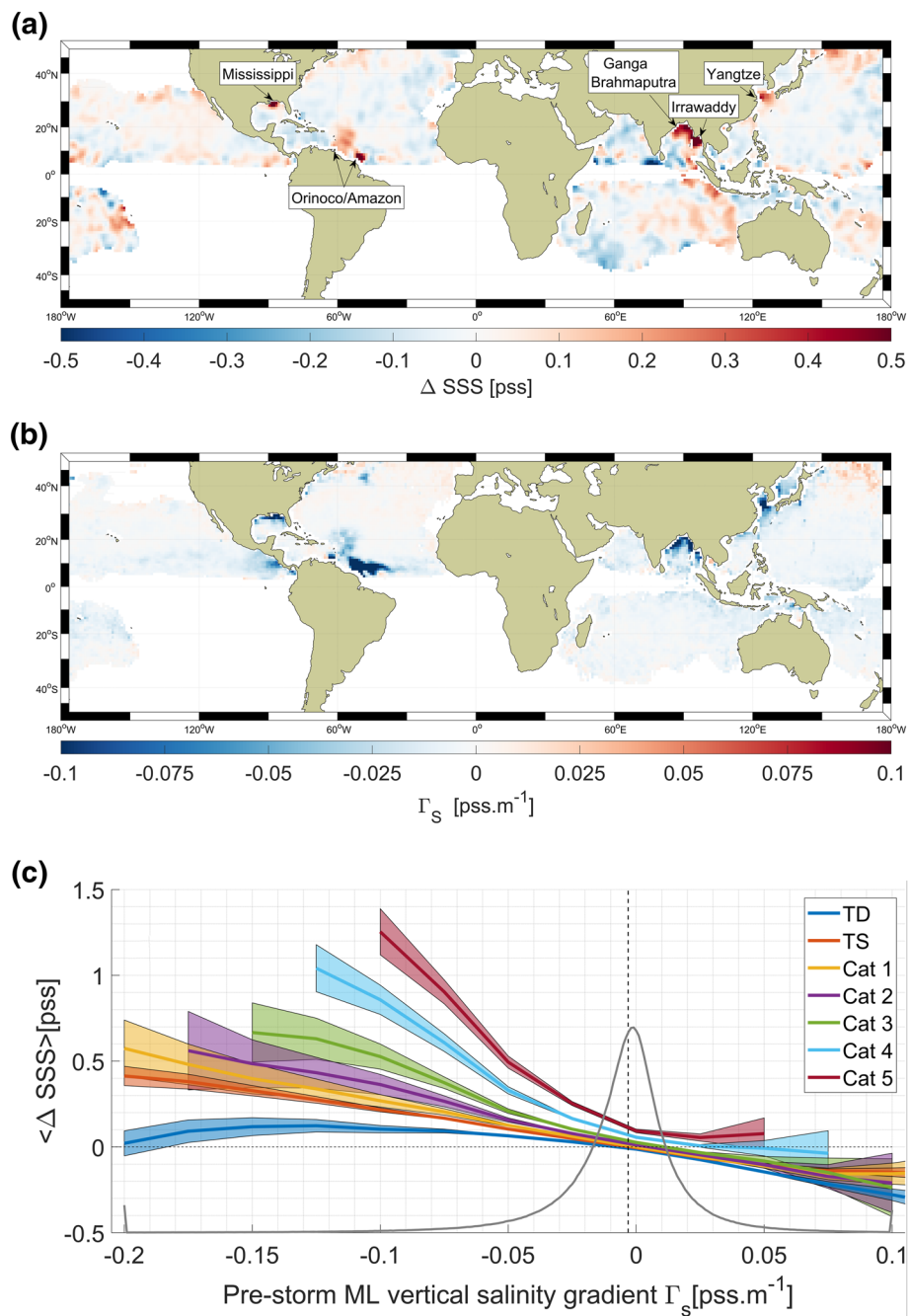


Figure 3. (a) Temporal average (2010–2019) of all storms SSS response in $1^\circ \times 1^\circ$ boxes. (b) Average prestorm mixed-layer vertical salinity gradient Γ_s in $1^\circ \times 1^\circ$ boxes. (c) Radially integrated (within $|r/R_{\max}| \leq 10$) SSS response to Tropical Cyclones bin-averaged as function of SSWS storm intensity (colors) and of Γ_s (x-axis, bin width of 0.025 pss/m). The gray curve and black dashed vertical line are the distribution of Γ_s (scaled to fit the graphic) and its median value, respectively. The color patches indicate the extent of the 95% confidence interval for the mean (thin black curves) in each bin. SSS, sea surface salinity; SSWS, Saffir-Simpson Wind Scale.

$\Gamma_s \geq 0$ ($\sim 40\%$ of the database), the TC-induced SSS anomalies are systematically negative (i.e., freshening) except for the most intense TCs (Categories 4–5), which are able to reach deeper and saltier waters.

The storm translation speed V_t is also known to significantly impact the ocean surface response to TCs (Kudryavtsev et al., 2019; Lloyd & Vecchi, 2011; Price, 1981). A nondimensional translation speed $\tau = \pi V_t / 4R_{\max} f$, with f the Coriolis parameter, is the ratio of local inertial period to the TC residence time.

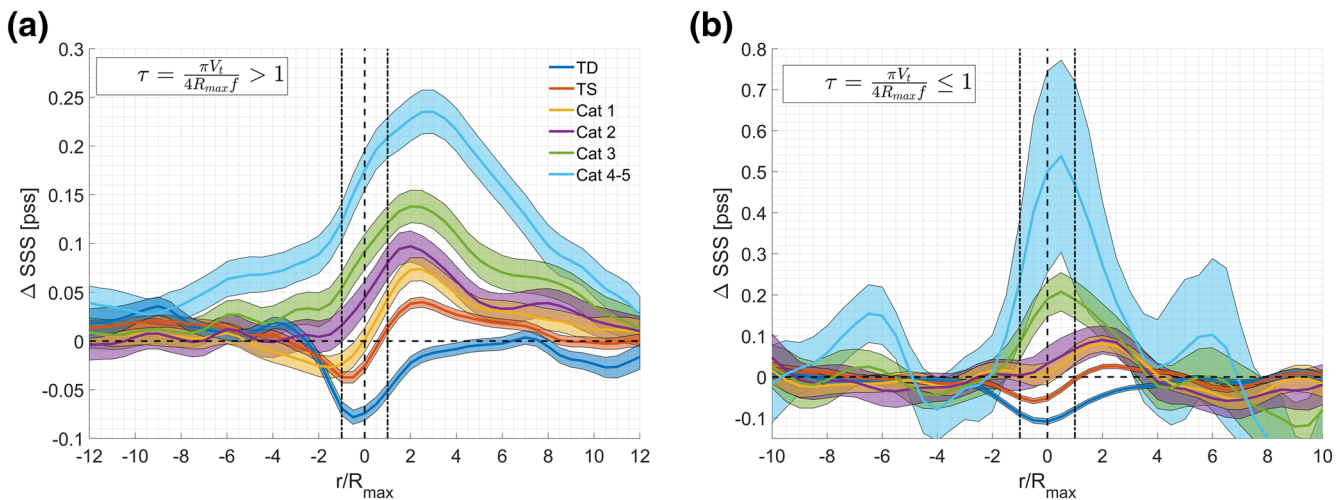


Figure 4. SSS response to TCs as functions of storm intensity for short (a, $\tau > 1$) and long (b, $\tau \leq 1$) storm residence time. For each intensity and radial distance bins, the mean (black curve) and the 95% confidence interval (color patch) are shown. SSS, sea surface salinity; TC, tropical cyclone.

It is confirmed in Figure 4 that areas of the ocean exposed to TCs for longer time intervals ($\tau < 1$) exhibit stronger poststorm salinity changes than for short residence times ($\tau > 1$). This is only evidenced for the most intense storms (Categories 3–5). Note that because of the high wind region masking in the level 2 satellite SSS, only 30% of the SSS anomaly data set is for long storm residence time $\tau < 1$, hence leading to increased uncertainties (95% confidence) in the median estimates in these conditions. The dynamic range of SSS response to TC intensity change from Tropical Depression to Category 4–5 force is found to be almost two times larger (0.4–0.8) for $\tau < 1$ than for $\tau > 1$ (~0.3–0.4). In addition, TC-induced salinification mostly extends within a narrow radial extent around the center ($|r/R_{\max}| < 4$) for long storm residence time. Salinification spreads radially within a much more extended domain ($|r/R_{\max}| < 12$) for fast moving storms, indicating the influence of cross-track advection by wind-driven currents. For instance, the maximum SSS response for the most intense storms (Categories 3–5) is significantly closer to the storm center (around $r/R_{\max} = 1$) for $\tau < 1$ than for $\tau > 1$ (around $r/R_{\max} = 2$).

Salt-stratified barrier layers (BLs) occur in oceanic regions where an upper ocean mixed-layer vertical salinity gradient Γ_s exists within an isothermal layer extending deeper than the MLD. As illustrated in Figure S4, when TCs pass over river plumes, or, rain-affected areas, prestorm BLs are, in general, thicker than 5 m. BLs in the tropical upper oceans can significantly influence TC intensification (Balaguru et al., 2012, 2020). They reduce vertical mixing efficiency, leading to less intense SST cooling, which can then impact TC evolution through changes in the air-sea enthalpy flux (Balaguru et al., 2012). Figure 3c confirms the influence of large prestorm ML salinity gradient Γ_s on ΔSSS , with saltier SSS responses. In the presence of thick BLs, we therefore expect reduced SST cooling and saltier SSS response after TC passage. This is clearly illustrated in Figure 5, where the median radial SST response to TCs as a function of intensity is significantly cooler for prestorm BLs thinner than 5 m (Figure 5c) compared to prestorm BLs thicker than 5 m (Figure 5d). The tendency is clearly opposite for the SSS response (Figures 5a, 5b, and S5): the thicker the BLs, the saltier the SSS response. Median SSS and SST responses over the full storm intensity SSWS range are ~0.25 psu and ~1.4 °C for BLT < 5 m, while they are ~0.5 psu and ~1 °C when BLT ≥ 5 m, respectively.

4. Summary and Conclusions

The climatological SSS response to Tropical Cyclones, after the wind forced stage, is determined for the first time at global scale using a decade of satellite data, combining observations from SMOS and SMAP missions. Consistent with reported rain-induced leftward asymmetric signatures of phytoplankton blooming in TC wakes (Lin & Oye, 2016), on the left (right) side of the Northern (Southern) Hemisphere storm center track and in the storm inner wall ($|r/R_{\max}| \leq 1$), SSS decreases for Tropical Depressions (~−0.1) and Tropical Storms (~−0.05).

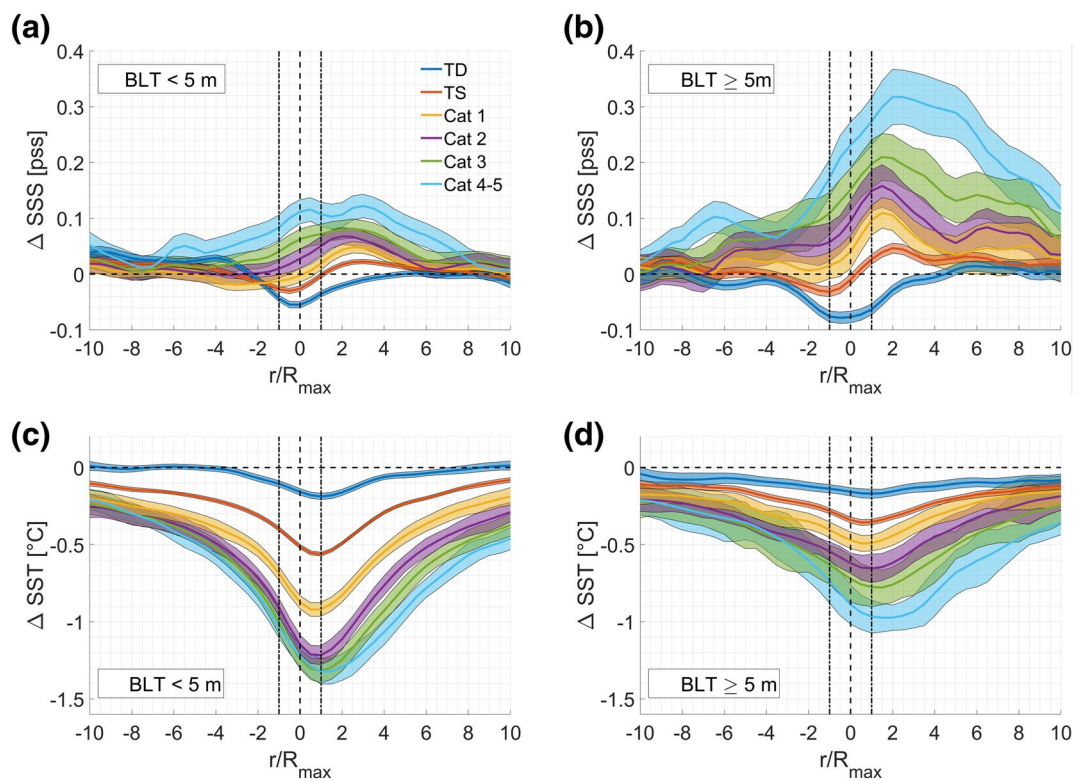


Figure 5. Radial (x-axes) distributions of the median relaxation stage SSS (a), (b) and SST (c), (d) responses to TC as function of intensity. In (a) and (c), the prestorm BL is thinner than 5 m while it is thicker than 5 m in (b) and (d) SSS, sea surface salinity; SST, sea surface temperature; TC, tropical cyclone.

Above hurricane force, passing TCs induce surface salinification, peaking rightward at around twice the maximum wind radius (Figure 2a) and extending almost everywhere within the extent of the Gale force wind region $|r/R_{34}| \leq 1$ (Figure S3b). The SSS wake is thus consistent with the SST wake (e.g., Figure 2b). The more intense the storm, the saltier the globally averaged SSS response to TCs (up to $\sim +1.5$ for the most intense storms, Figure 3c).

From this global analysis, strong regional variability emerges for the net impact of all TCs on SSS. There are areas dominated by mixed-layer freshening following Tropical Depression and Storm passage (Arabian Sea, southern tip of India, north of Australia, most of the western Pacific, Atlantic north of 20°N, Caribbean Sea, Southwest Indian Ocean). But striking impacts of TCs on SSS are found where mixing of fresh surface river plumes with saltier subsurface waters (Amazon, Orinoco, Mississippi, Bay of Bengal, Pearl, and Yangtze) occurs.

The prestorm vertical salinity gradient in the upper ocean mixed-layer Γ_s is thus a key driver of this strong regional variability in the SSS responses to TCs. As expected from TC-induced mixing and upwelling effects, when $\Gamma_s < 0$ (stable stratification), the fresher the prestorm SSS with respect the prestorm salinity just below the MLD, the saltier the SSS response at a fixed TC intensity.

This dependency of the haline response is further modulated by the nondimensional storm translation speed τ (ratio of local inertial period to the TC residence time). The change in SSS response as TC intensity changes from Tropical Depression to Category 4–5 force is found almost two times larger (0.4–0.8) for storms with long residence time $\tau < 1$, than it is for short storm residence time $\tau > 1$ (~ 0.3 –0.4). Comparable to the proposed scaling of the SST changes (e.g., Kudryavtsev et al., 2019, their Equations 8 and 10), the haline surface response to TCs is therefore dependent on at least the storm intensity (V_{\max}), normalized radial distance from the storm track (r/R_{\max}), strength of the prestorm vertical salinity gradient in the upper ocean mixed-layer Γ_s , the Brunt-Väisälä parameter N evaluated in the upper seasonal thermocline layer,

and nondimensional storm translation speed τ : $\Delta SSS = \text{functional}(V_{\max}, r/R_{\max}, \Gamma_s, N, \tau)$. Consistent with previous statistical analyses based on either model results at global scale (Jourdain et al., 2013), or Argo float data in the Northwest Pacific (Lin et al., 2017), SMOS and SMAP SSS data reveal that on average, the mixing effect overwhelms the dilution effect of rain. An important factor for ΔSSS variability that was not studied here is the impact of the local freshwater atmospheric forcing budget. The balance between TC-induced evaporation and precipitation (E-P) certainly impacts the reported median SSS responses. Investigating ΔSSS dependencies to include E-P radial distribution is left for future investigations. Reported effects of vertical wind shear on TC rainfall asymmetries (Chen et al., 2006) might indeed also impact the SSS-response radial distribution. Nevertheless, the present analysis already confirms that in the presence of weak prestorm vertical ML salinity gradients, SSS median responses to hurricane force TCs are mostly positive (Figure 3c). Precipitation effects may thus only lower the average SSS response to the most intense TCs.

The present analysis also emphasizes the influences of salt-stratified barrier layers. As anticipated and unambiguously revealed, SSS and SST responses to TCs do not behave similarly in such conditions. In particular, we found reduced SST cooling and increased SSS salinification after the passage of TCs over thick BLs. To first-order, satellite SSS can thus inform about the expected resulting strength of hurricane-induced mixing and upwelling, and should be incorporated into metrics of TC-induced SST cooling (e.g., Balaguru et al., 2015; Price, 2009; Reul et al., 2014; Shay & Brewster, 2010; Vincent et al., 2012). The available 10-years period of satellite salinity should further be considered to study statistical prediction of TC rapid intensification. Although TCs are relatively short-lived (~ 10 days), given the TC locations over major surface freshwater pools of tropical and subtropical oceans, TC-induced surface salinification and subsurface freshening may be significant modulators of the long-term variability of the upper ocean static stratification.

Data Availability Statement

SMOS L3OS 2Q products are available at the Centre Aval de Traitement des Données SMOS at <https://www.catds.fr/>. SMAP salinity products V4.0 are available at Remote Sensing Systems at www.remss.com/missions/smap/. (GHRSSST) Level 4 Global Foundation Sea Surface Temperature analysis v5.0 are available at https://podaac.jpl.nasa.gov/dataset/MW_IR_OI-REMSS-L4-GLOB-v5.0. In Situ Analysis System (ISAS-15) data are available at <https://www.seanoe.org/data/00412/52367/>.

Acknowledgments

The authors would like to thank two anonymous reviewers. This work was supported by the CNES-TOSCA "SMOS Ocean" and ESA "Level 2 OS" and "CCI-SSS" projects. V. Kudryavtsev and B. Chapron gratefully acknowledge support of the Russian Science Foundation through the grant 17-77-30019.

References

- Balaguru, K., Chang, P., Saravanan, R., Leung, L. R., Xu, Z., Li, M., et al. (2012). Ocean barrier layers' effect on tropical cyclone intensification. *Proceedings of the National Academy of Sciences of the United States of America*, 109(36), 14343–14347.
- Balaguru, K., Foltz, G. R., Leung, L. R., Asaro, D. E., Emanuel, K. A., Liu, H., et al. (2015). Dynamic potential intensity: An improved representation of the ocean's impact on tropical cyclones. *Geophysical Research Letters*, 42, 6739–6746. <https://doi.org/10.1002/2015GL064822>
- Balaguru, K., Foltz, G. R., Leung, L. R., Kaplan, J., Xu, W., Reul, N., et al. (2020). Pronounced impact of salinity on rapidly intensifying tropical cyclones. *Bulletin of the American Meteorological Society*, 101(9), E1497–E1511. <https://doi.org/10.1175/BAMS-D-19-0303.1>
- Bond, N. A., Cronin, M. F., Sabine, C., Kawai, Y., Ichikawa, H., Freitag, P., et al. (2011). Upper ocean response to Typhoon Choi-Wan as measured by the Kuroshio Extension Observatory mooring. *Journal of Geophysical Research: Oceans*, 116, C02031. <https://doi.org/10.1029/2010JC006548>
- Boutin, J., Vergely, J. L., Marchand, S., D'Amico, F., Hasson, A., Kolodziejczyk, N., et al. (2018). New SMOS sea surface salinity with reduced systematic errors and improved variability. *Remote Sensing of Environment*, 214, 115–134. <https://doi.org/10.1016/j.rse.2018.05.022>
- CATDS (2019). CATDS-PDC L3OS 2Q—Debiased Daily Valid Ocean Salinity Values Product from SMOS Satellite. CATDS (CNES, IFREMER, LOCEAN, ACRI). <http://dx.doi.org/10.12770/12dba510-cd71-4d4f-9fc1-9cc027d128b0>
- Chaudhuri, D., Sengupta, D., D'Asaro, E., Venkatesan, R., & Ravichandran, M. (2019). Response of the salinity-stratified Bay of Bengal to cyclone Phailin. *Journal of Physical Oceanography*, 49, 1121–1140. <https://doi.org/10.1175/JPO-D-18-0051.1>
- Chen, S. S., Knaff, J. A., & Marks, F. D. Jr. (2006). Effects of vertical wind shear and storm motion on tropical cyclone rainfall asymmetries deduced from TRMM. *Monthly Weather Review*, 134(11), 3190–3208. <https://doi.org/10.1175/MWR3245.1>
- De Boyer Montégut, C., Mignot, J., Lazar, A., & Cravatte, S. (2007). Control of salinity on the mixed layer depth in the world ocean: 1. General description. *Journal of Geophysical Research: Oceans*, 112, C06011. <https://doi.org/10.1029/2006JC003953>
- Domingues, R., Goni, G., Bringas, F., Lee, S.-K., Kim, H.-S., Halliwell, G., et al. (2015). Upper ocean response to Hurricane Gonzalo (2014): Salinity effects revealed by targeted and sustained underwater glider observations. *Geophysical Research Letters*, 42, 7131–7138. <https://doi.org/10.1002/2015GL065378>
- Entekhabi, D., Yueh, S., O'Neill, P. E., Kellogg, K. H., Allen, A., Bindlish, R., et al. (2014). SMAP Handbook (JPL 400-1567). Pasadena, CA: Jet Propulsion Laboratory. https://smap.jpl.nasa.gov/system/internal_resources/details/original/178_SMAP_Handbook_FINAL_1_JULY_2014_Web.pdf

- Gaillard, F., Reynaud, T., Thierry, V., Kolodziejczyk, N., & Von Schuckmann, K. (2016). In-situ based reanalysis of the global ocean temperature and salinity with ISAS: Variability of the heat content and steric height. *Journal of Climate*, 29(4), 1305–1323. <https://doi.org/10.1175/JCLI-D-15-0028.1>
- Ginis, I. (2002). Tropical cyclone-ocean interactions, in atmosphere ocean interactions. *Advances in Fluid Mechanics Series*, 33, 83–114.
- Grodsky, S. A., Reul, N., Lagerloef, G., Reverdin, G., Carton, J. A., Chapron, B., et al. (2012). Haline hurricane wake in the Amazon/Orinoco plume: AQUARIUS/SACD and SMOS observations. *Geophysical Research Letters*, 39, L20603. <https://doi.org/10.1029/2012GL053335>
- Hall, T. M., & Kossin, J. P. (2019). Hurricane stalling along the North American coast and implications for rainfall. *npj Climate and Atmospheric Science*, 2, 17. <https://doi.org/10.1038/s41612-019-0074-8>
- Hsu, P., & Ho, C. (2019). Typhoon-induced ocean subsurface variations from glider data in the Kuroshio region adjacent to Taiwan. *Journal of Oceanography*, 75, 1–21. <https://doi.org/10.1007/s10872-018-0480-2>
- Jacob, S. D., & Koblinsky, C. J. (2007). Effects of precipitation on the upper-ocean response to a hurricane. *Monthly Weather Review*, 135, 2207–2225. <https://doi.org/10.1175/MWR3366.1>
- Jourdain, N. C., Lengaigne, M., Vialard, J., Madec, G., Menkes, C., Vincent, E. M., et al. (2013). Observation-based estimates of surface cooling inhibition by heavy rainfall under tropical cyclones. *Journal of Physical Oceanography*, 43(1), 205–221. <https://doi.org/10.1175/JPO-D-12-0851>
- Kerr, Y. H., Waldteufel, P., Wigneron, J.-P., Delwart, S., Cabot, F., Boutin, J., et al. (2010). The SMOS mission: New tool for monitoring key elements of the global water cycle. *Proceedings of the IEEE*, 98(5), 666–687. <https://doi.org/10.1109/JPROC.2010.2043032>
- Kil, B., Burrage, D., Wesson, J., & Howden, S. (2013). Sea surface signature of tropical cyclones using microwave remote sensing. *Proceedings of SPIE—The International Society for Optical Engineering*, 8724, 1–15.
- Knaff, J. A., Longmore, S. P., & Molnar, D. A. (2014). An objective satellite-based tropical cyclone size climatology. *Journal of Climate*, 27, 455–476. <https://doi.org/10.1175/JCLI-D-13-00096.1>
- Knapp, K. R., Kruk, M. C., Levinson, D. H., Diamond, H. J., & Neumann, C. J. (2010). The International Best Track Archive for Climate Stewardship (IBTrACS): Unifying tropical cyclone best track data. *Bulletin of the American Meteorological Society*, 91, 363–376. <https://doi.org/10.1175/2009BAMS2755.1>
- Kudryavtsev, V., MonzikovaCombó, A. C., Chapron, B., & Reul, N. (2019). A simplified model for the baroclinic and barotropic ocean response to moving tropical cyclones: 2. Model and simulations. *Journal of Geophysical Research: Oceans*, 124, 3462–3485. <https://doi.org/10.1029/2018JC014747>
- Lin, Y.-C., & Oey, L.-Y. (2016). Rainfall-enhanced blooming in typhoon wakes. *Scientific Reports*, 6, 31310. <https://doi.org/10.1038/srep31310>
- Lin, S., Zhang, W., Shang, S., & Hong, H. (2017). Ocean response to typhoons in the western North Pacific: Composite results from Argo data. *Deep Sea Research Part I: Oceanographic Research Papers*, 123, 62–74. <https://doi.org/10.1016/j.dsr.2017.03.007>
- Liu, F., Zhang, H., Ming, J., Zheng, J., Tian, D., & Chen, D. (2020). Importance of precipitation on the upper ocean salinity response to typhoon Kalmaegi(2014). *Water*, 12, 614. <https://doi.org/10.3390/w12020614>
- Liu, Z., Xu, J., Zhu, B., Sun, C., & Zhang, L. (2007). The upper ocean response to tropical cyclones in the northwestern Pacific analyzed with Argo data. *Chinese Journal of Oceanology and Limnology*, 25, 123–131. <https://doi.org/10.1007/s00343-007-0123-8>
- Lloyd, I. D., & Vecchi, G. A. (2011). Observational evidence for oceanic controls on hurricane intensity. *Journal of Climate*, 24, 1138–1153. <https://doi.org/10.1175/2010JCLI3763.1>
- McPhaden, M. J., Foltz, G. R., Lee, T., Murty, V. S. N., Ravichandran, M., Vecchi, G. A., et al. (2009). Ocean-atmosphere interactions during cyclone Nargis. *EOS, Transactions American Geophysical Union*, 90, 53–54. <https://doi.org/10.1029/2009EO070001>
- Meissner, T., Wentz, F. J., & Manaster, A. (2018). *Remote Sensing Systems SMAP Ocean Surface Salinities (Level 2C, Level 3 Running 8-day, Level 3 Monthly)*. Santa Rosa, CA: Remote Sensing Systems. <https://doi.org/10.5067/SMP3A-2SOC5>
- Neethu, C. (2018). Insights into the haline variability induced by cyclone Vardah in the Bay of Bengal using SMAP salinity observations. *Remote Sensing Letters*, 9(12), 1205–1213. <https://doi.org/10.1080/2150704X.2018.1519271>
- Price, J. F. (1981). Upper ocean response to a hurricane. *Journal of Physical Oceanography*, 11, 153–175. [https://doi.org/10.1175/1520-0485\(1981\)0112.0.CO;2](https://doi.org/10.1175/1520-0485(1981)0112.0.CO;2)
- Price, J. F. (2009). Metrics of hurricane-ocean interaction: Vertically-integrated or vertically-averaged ocean temperature? *Ocean Science*, 5, 351–368. <https://doi.org/10.5194/os-5-351-2009>
- Pudov, V. D., & Petrenchenko, S. A. (2000). Trail of a typhoon in the salinity field of the ocean upper layer. *Atmospheric and Ocean Physics (Izvestiya Atmospheric and Oceanic Physics)*, 36, 645–650.
- Remote Sensing Systems (2017). *GHRSST Level 4 MW_IR_OI Global Foundation Sea Surface Temperature Analysis Version 5.0 from REMSS, Ver: 5.0*. CA: PO.DAAC Dataset accessed [2019-02-15] at <https://doi.org/10.5067/GHMWI-4FR05>
- Reul, N., Grodsky, S. A., Arias, M., Boutin, J., Catany, R., Chapron, B., et al. (2020). Sea surface salinity estimates from spaceborne L-band radiometers: An overview of the first decade of observation (2010–2019). *Remote Sensing of Environment*, 242, 111769. <https://doi.org/10.1016/j.rse.2020.111769>
- Reul, N., Quilfen, Y., Chapron, B., Fournier, S., Kudryavtsev, V., & Sabia, R. (2014). Multisensor observations of the Amazon-Orinoco river plume interactions with hurricanes. *Journal of Geophysical Research: Oceans*, 119, 8271–8295. <https://doi.org/10.1002/2014JC010107>
- Robertson, E. J., & Ginis, I. (2002). The Upper Ocean Salinity Response to Tropical Cyclones. Preprints, 25th Conference on Hurricanes and Tropical Meteorology (14D. 5). San Diego, CA: American Meteorological Society.
- Sanford, T. B., Black, P. G., Haustein, J. R., Feeney, J. W., Forristall, G. Z., & Price, J. F. (1987). Ocean response to a hurricane. Part I: Observations. *Journal of Physical Oceanography*, 17, 2065–2083. [https://doi.org/10.1175/1520-0485\(1987\)017%3C2065:ORTAHP%3E2.0.CO;2](https://doi.org/10.1175/1520-0485(1987)017%3C2065:ORTAHP%3E2.0.CO;2)
- Schott, T., Landsea, C., Hafele, G., Lorens, J., Taylor, A., Thurm, H., et al. (2012). The Saffir-Simpson Hurricane Wind Scale. *National Weather Services, National Hurricane Centre, National Oceanic and Atmospheric Administration (NOAA) Factsheet*. <http://www.nhc.noaa.gov/pdf/sshws.pdf>
- Shay, L. K., & Brewster, J. K. (2010). Eastern Pacific oceanic heat content estimation for hurricane intensity forecasting. *Monthly Weather Review*, 138, 2110–2131. <https://doi.org/10.1175/2010MWR3189.1>
- Steffen, J., & Bourassa, M. (2018). Barrier layer development local to tropical cyclones based on Argo float observations. *Journal of Physical Oceanography*, 48, 1951–1968. <https://doi.org/10.1175/JPO-D-17-0262.1>
- Venkatesan, R., Mathew, S., Vimala, J., Latha, G., Muthiah, A., Ramasundaram, S., et al. (2014). Signatures of very severe cyclonic storm Phailin in met-ocean parameters observed by moored buoy network in the Bay of Bengal. *Current Science*, 107(4), 589–595. <https://www.jstor.org/stable/24103530>
- Vinayachandran, P. N., & Mathew, S. (2003). Phytoplankton bloom in the Bay of Bengal during northeast monsoon and its intensification by cyclones. *Geophysical Research Letters*, 30(11), 1572. <https://doi.org/10.1029/2002GL016717>

- Vincent, E. M., Lengaigne, M., Vialard, J., Madec, G., Jourdain, N. C., & Masson, S. (2012). Assessing the oceanic control on the amplitude of sea surface cooling induced by tropical cyclones. *Journal of Geophysical Research: Oceans*, 117, C05023. <https://doi.org/10.1029/2011JC007705>
- Yue, X., Zhang, B., Liu, G., Li, X., Zhang, H., & He, Y. (2018). Upper ocean response to typhoon Kalmaegi and Sarika in the South China sea from Multiple-satellite observations and numerical simulations. *Remote Sensing*, 10, 348. <https://doi.org/10.3390/rs10020348>
- Zhang, H., Chen, D., Zhou, L., Liu, X., Ding, T., & Zhou, B. (2016). Upper ocean response to typhoon Kalmaegi (2014). *Journal of Geophysical Research: Oceans*, 121, 6520–6535. <https://doi.org/10.1002/2016JC012064>
- Zhang, Z., Wu, H., Yin, X., & Qiao, F. (2018). Dynamical response of Changjiang River plume to a severe typhoon with the surface wave-induced mixing. *Journal of Geophysical Research: Oceans*, 123, 9369–9388. <https://doi.org/10.1029/2018JC014266>

References From the Supporting Information

- Dare, R. A., & McBride, J. L. (2011). Sea surface temperature response to tropical cyclones. *Monthly Weather Review*, 139, 3798–3808 <https://doi.org/10.1175/MWR-D-10-05019.1>
- Schumacher, R. S., Galarraga, T. J., & Bosart, L. F. (2011). Distant effects of a recurring tropical cyclone on rainfall in a midlatitude convective system: A high-impact predecessor rain event. *Monthly Weather Review*, 139, 650–667 <https://doi.org/10.1175/2010MWR3453.1>
- Vincent, E. M., Lengaigne, M., Madec, G., Vialard, J., Samson, G., Jourdain, N. C., et al (2012). Processes setting the characteristics of sea surface cooling induced by tropical cyclones. *Journal of Geophysical Research: Oceans*, 117, C02020 <http://dx.doi.org/10.1029/2011JC007396>
- Wang, X.-D., Han, G., Qi, Y.-Q., & Li, W. (2011). Impact of barrier layer on typhoon-induced sea surface cooling. *Dynamics of Atmospheres and Oceans*, 52, 367–385 <https://doi.org/10.1016/j.damatmoce.2011.05.002>
- Wang, Y., Wang, Y., & Fudeyasu, H. (2009). The role of Typhoon Songda (2004) in producing distantly located heavy rainfall in Japan. *Monthly Weather Review*, 137, 3699–3716 <https://doi.org/10.1175/2009MWR2933.1>